Measurement of the gravitational potential evolution from the cross-correlation between WMAP and the APM Galaxy survey

Pablo Fosalba[1], Enrique Gaztañaga[2]

[1]*Institut d'Astrophysique de Paris, 98bis Bd Arago, 75014 Paris, France*
[2]*Institut d'Estudis Espacials de Catalunya. IEEC/CSIC, Gran Capitán 2-4, 08034 Barcelona, Spain*

Cosmological models with late time cosmic acceleration, such as the Λ-dominated FRW model, predict a freeze out for the gravitational growth of large scale (linear) dark-matter fluctuations at moderate redshift $z < 1$. This leaves an imprint on the dynamics of the gravitational potential that can be observed as temperature fluctuations in the CMB: the so called integrated Sachs-Wolfe (ISW) effect. We present a direct measurement of the ISW effect based on the angular cross-correlation function, $w_{TG}(\theta) = \langle \Delta T \delta_G \rangle$, of CMB temperature anisotropies ΔT, and dark-matter fluctuations traced by galaxies δ_G. We use the best current data to trace such anisotropies: the first-year WMAP data in combination with the APM Galaxy survey. On the largest scales, $\theta = 5 - 10$ deg, our analysis yields $w_{TG} = 0.35 \pm 0.20 \mu K$ (90% C.L.), what favors large values of $\Omega_\Lambda = 0.3 - 0.8$ for flat FRW models. The measured cross-correlation is slightly larger, but in good agreement with recent analysis based on X-ray and radio sources [6], [24]. On smaller scales, $\theta < 1$deg one expects a comparable ISW contribution. Instead we find a negative correlation $w_{TG} = -0.2 \pm 0.2 \mu K$. Although such scales are dominated by sampling variance, our analysis clearly indicates a cancellation of ISW with inverse Compton scattering in the hot gas in galaxy clusters, ie the thermal Sunyaev-Zeldovich (SZ) effect. The SZ contribution is $w_{TG} = -0.5 \pm 0.2 \pm 0.2 \mu K$ (90% C.L.), which can be used to set new limits on the total mean Compton distortion of CMB photons.

I. INTRODUCTION

We cross-correlation of the cosmic microwave background (CMB) anisotropies measured by WMAP [3], with the matter density fluctuations as traced by galaxies in the APM Galaxy Survey [22]. The recent measurements of CMB anisotropies made public by the WMAP team are in good agreement with a 'concordance' cosmology based on the ΛCDM model. The unprecedented sensitivity, frequency and sky coverage, of this new data set provides us the opportunity of asking new questions about the evolution of the universe.

The APM Survey has produced one of the best estimates of the angular galaxy 2-point correlation function to date. Its shape on large scales led to the discovery of excess large-scale power, and gave early indications of the ΛCDM model [10], [22], [1], [15]. Higher-order correlations have also been studied in the APM Galaxy Survey [16], [33], [12]. For the first time, these measurements were accurate enough and extended to sufficiently large scales to probe the weakly non-linear regime with a reliable Survey. The results are in good agreement with gravitational growth for a model with initial Gaussian fluctuations. They also indicate that the APM galaxies are relatively unbiased tracers of the mass on large scales [18]), and provide stringent constraints upon models with non-Gaussian initial conditions. Moreover the APM results are in excellent agreement with other wide field photometric surveys, such as the Sloan Digital Sky Survey (SDSS), for both number counts and clustering (see e.g. [9], [30], [13], [14]).

II. DATA $ SIMULATIONS

The APM Galaxy Survey [22] is based on 185 UK IIIA-J Schmidt photographic plates each corresponding to 5.8×5.8 deg^2 on the sky limited to $b_J \simeq 20.5$ and having a mean depth of $\simeq 400$ Mpc/h for $b < -40$ deg and $\delta < -20$ deg. These fields where scanned by the APM machine and carefully matched using the 5.8×0.8 deg^2 plate overlaps. Out of the APM Survey we considered a $17 < b_J < 20$ magnitude slice in an equal-area projection pixel map with a resolution of $3.5'$, that covers over 4300 deg^2 around the SGC.

We use the full-sky CMB maps from the first-year WMAP data [3]. In particular, we have chosen the V-band (~ 61 GHz) for our analysis since it has a lower pixel noise than the highest frequency W-band (~ 94 GHz), while it has sufficiently high spatial resolution ($21'$) for our purposes. We mask out pixels using the most conservative mask, the so-called Kp0 mask, what cuts 21.4% of sky pixels [4], to make sure Galactic emission does not affect our analysis. WMAP and APM data is digitized into $6.9'$ pixels using the Healpix tesselation ($N_{side} = 512$) on the sphere [20]. Figs 1 show these maps smoothed using a Gaussian beam of FWHM $= 5°$ and FWHM $= 0.7°$.

In order to determine whether we detect a significant WMAP-APM cross-correlation (see §III below) we compute the associated null-test error bars by running 30 WMAP V-band Monte-Carlo realizations. For this purpose we simulate the signal by making random realizations of the CMB angular power-spectrum C_ℓ as measured by WMAP to which we add random realizations of the white noise estimated for the V-band [21]. Sampling variance in the WMAP-APM cross-correlation is
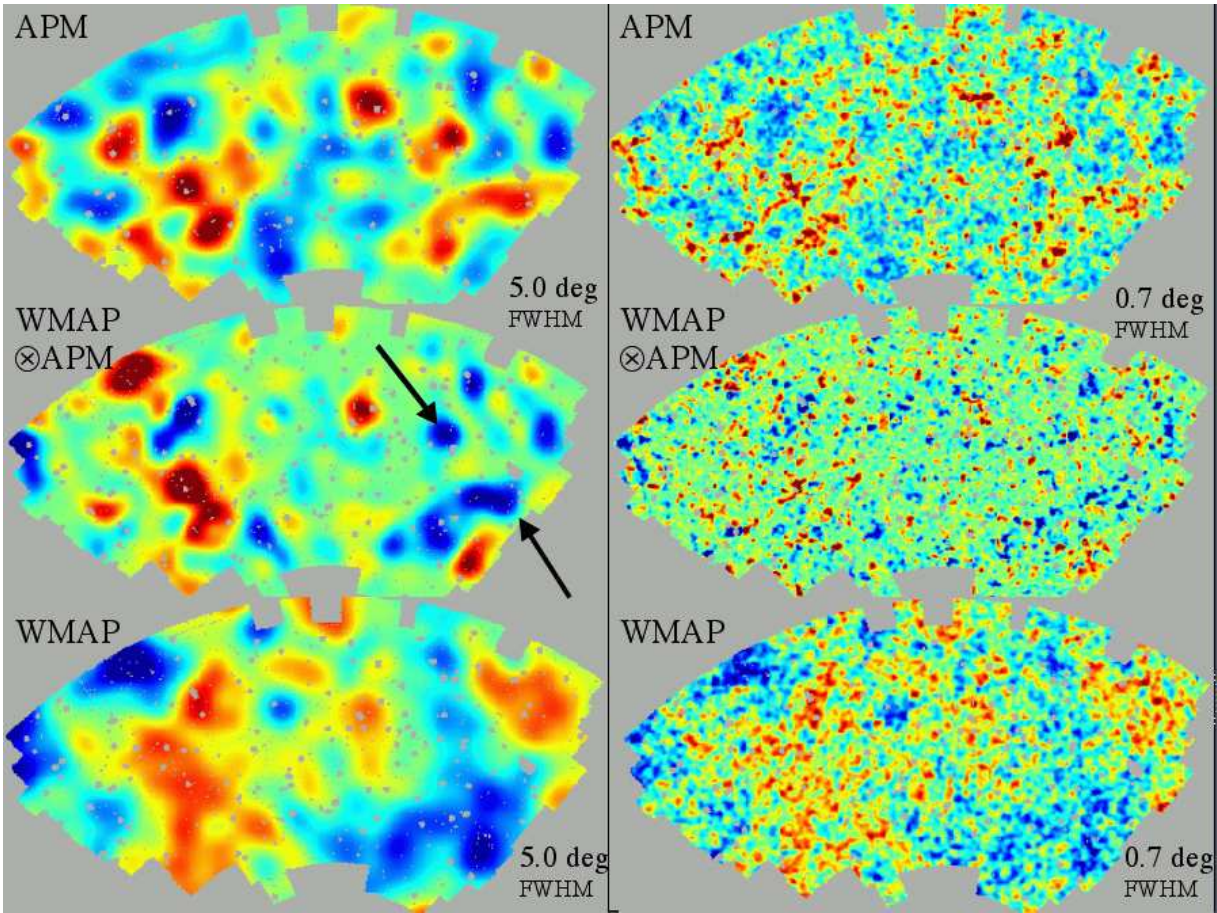
FIG. 1: APM galaxy density fluctuation maps (top panels) compared to WMAP (V-band) maps (bottom panels) and the cross-correlation map (middle). In each case left panels show the maps smooth with a Gaussian beam of FWHM = 5° while right panels have FWHM = 0.7°. We use normalized units (dimensionless) with linear color scheme in the range $(-3\sigma, +3\sigma)$, being σ the pixel variance in each map.

thus evaluated by computing the correlation between the simulated V-band CMB maps (with WMAP Kp0 mask pixels removed) with the APM survey. Note that this approach is conservative because the WMAP C_ℓ include all the power on the sky, including the power from secondary fluctuations that correlate with the APM. In the simulations such source of extra power acts as an additional source of noise, while in the actual (WMAP) CMB map this is the signal that potentially correlates with the APM and that we aim at measuring.

III. WMAP-APM CROSS-CORRELATION

We define the cross-correlation function as the expectation value of density fluctuations $\delta_G = N_G / <N_G> -1$ and temperature anisotropies $\Delta_T = T - T_0$ (in μK) at two positions $\hat{n}_1$ and $\hat{n}_2$ in the sky:

$$w_{TG}(\theta) \equiv \langle \Delta_T(\hat{\mathbf{n}}_1)\delta_G(\hat{\mathbf{n}}_2)\rangle, \qquad (1)$$

where $\theta = |\hat{\mathbf{n}}_2 - \hat{\mathbf{n}}_1|$, assuming that the distribution is statistically isotropic. To estimate $w_{TG}(\theta)$ from the pixel maps we use:

$$w_{TG}(\theta) = \frac{\sum_{i,j} \Delta_T(\hat{\mathbf{n}}_\mathbf{i})\, \delta_G(\hat{\mathbf{n}}_\mathbf{j})\, w_i\, w_j}{\sum_{i,j} w_i\, w_j}, \qquad (2)$$

where the sum extends to all pairs i, j separated by $\theta \pm \Delta\theta$. The mean temperature fluctuation is subtracted so that $\langle \delta_i \rangle = 0$. The weights w_i can be used to minimize the variance when the pixel noise is not uniform, however this introduces larger cosmic variance. Here we follow the WMAP team and use uniform weights (i.e. $w_i = 1$). We consider angular scales, $\theta < 10°$. Cross-correlations are expected to be dominated by sampling variance beyond $\sim 10°$, where the APM angular correlation function vanishes and we only have a few independent subregions of size $> 10°$. Fig 2 shows the resulting cross-correlation with constant bin $\Delta\theta = 0.2$. On scales above $\theta > 5$ deg there is a significant correlation above the estimated error-bars.

Fig 3 shows the 1-σ confidence interval for $w_{TG}(\theta)$ estimation obtained using the jack-knife covariance matrix. Surveys are first divided into M separate regions on the
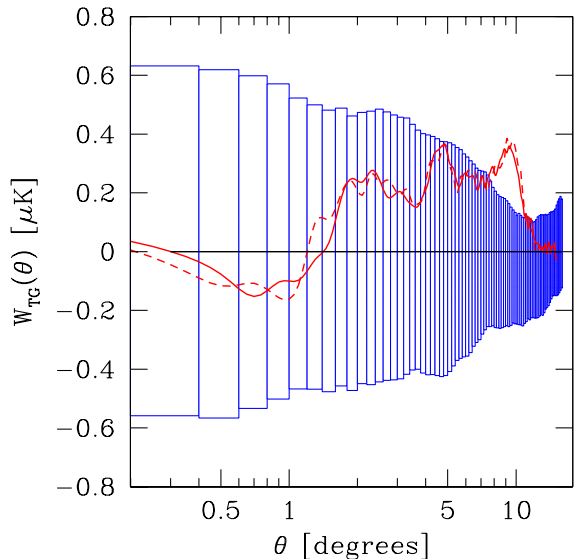
FIG. 2: Measured cross-correlation $w_{TG}(\theta)$ between WMAP and APM as a function of angular separation. Continuous and dashed lines show the results for WMAP V and W-bands, respectively. Error-bars correspond to the rms dispersion in the null-test of correlating APM with 30 WMAP simulations.

sky, each of equal area. The analysis is then performed M times, each time removing a different region, the so-called jack-knife subsamples, which we label $k = 1 \dots M$. The estimated statistical covariance for w_{TG} at scales θ_i and θ_j is then given by:

$$C_{ij} = \frac{M-1}{M} \sum_{k=1}^{M} \Delta w_{TG}^k(\theta_i) \Delta w_{TG}^k(\theta_j) \qquad (3)$$

$$\Delta w_{TG}^k(\theta_i) \equiv w_{TG}^k(\theta_i) - \widetilde{w_{TG}}(\theta_i) \qquad (4)$$

where $w_{TG}^k(\theta_i)$ is the measure in the k-th jack-knife subsample ($k = 1 \dots M$) and $\widetilde{w_{TG}}(\theta_i)$ is the mean value for the M subsamples. The case $i = j$ gives the error variance. Note how, if we increase the number of regions M, the jack-knife subsamples are larger and each term in the sum is smaller. We take $M = 8$ so that each region is large enough to include a few structures at the largest scale considered (i.e a fair sample). The accuracy of the jack-knife covariance have been tested for both WMAP [19] and the APM and SDSS survey [30], [14], [13].

We can now estimate confidence regions in w_{TG} using a χ^2 test:

$$\chi^2 = \sum_{i,j=1}^{N} \Delta_i \ C_{ij}^{-1} \ \Delta_j, \qquad (5)$$

where $\Delta_i \equiv w_{TG}^O(\theta_i) - w_{TG}^M(\theta_i)$ is the difference between the "observation" O and the model M. The model can be either predictions or a mean estimation. To eliminate the degeneracies in the covariance matrix, we perform a
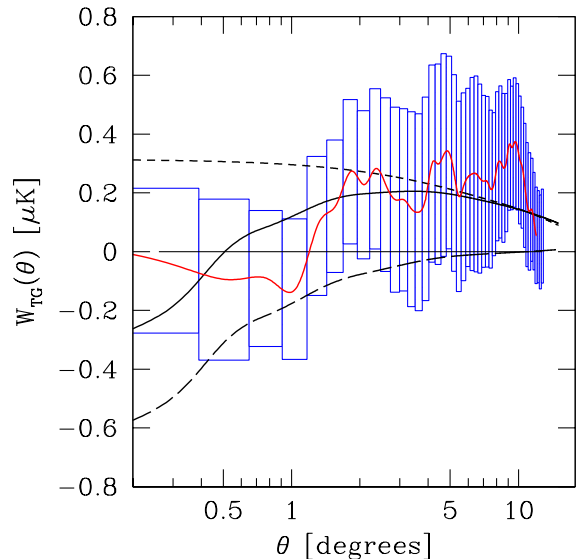

FIG. 3: Shaded region shows the cross-correlation $w_{TG}(\theta)$ of WMAP with APM galaxy fluctuations and the symmetrized 68% confidence levels obtained from a χ^2 fit using the jack-knife covariance matrix. Short-dashed, long-dashed and continuous lines show theoretical predictions for ISW, SZ and their sum, respectively.

Singular Value Decomposition (SVD) of the matrix and select only the largest modes to include in our χ^2. We can then fit predictions or estimations by requiring a minimum χ^2. Confidence levels (C.L.) are obtained for values relative to the minimum χ^2. Fig 3 shows the symmetrized 68% confidence regions in the mean w_{TG} estimation with constant bin $\Delta\theta = 0.26$. Note how on large scales $\theta > 5$ deg jack-knife errors are comparable to the conservative null-test errors in Fig 2, while on smaller scales, where jack-knife errors are more reliable, they are up to $2 - 3$ times smaller. This indicates that the small scale signal is quite homogeneous over the entire APM-WPAM map (see middle right panel in Fig 1), more so than expected in simulations. As mentioned above this is an indication that the cross-correlation signal artificially increases the noise in the simulations.

A. Comparison with Predictions

Galaxy fluctuations in the sky can be modeled as:

$$\delta_G(\hat{n}) = \int dz \ \phi_G(z) \ \delta_G(\hat{n}, z). \qquad (6)$$

where $\phi_G(z)$ models the survey selection function along the line-of-sight. We will assume here that APM galaxies are good tracers of the mass on large scales (see §I), so that we can use the linear bias relation: $\delta_G \simeq b\delta$, with $b \simeq 1$ and for the power spectrum: $P_G(k, z) \simeq b(z)^2 P(k, z)$. In the linear regime we further have:

$P(k, z) = D^2(z) P(k)$. We can then define a galaxy window function $W_G(z) \simeq b(z) D(z) \phi_G(z)$ that accounts for biasing, linear growth, and the galaxy selection function. The galaxy 2-point angular correlation $w_{GG}(\theta)$ is then (e.g. [1], [17]):

$$w_{GG}(\theta) = < \delta_G \delta_G > = \int dk \; k \; P(k) \; g_G(k\,\theta) \; . \quad (7)$$

The kernel $g_G(k\,\theta)$ is an integral along the line-of-sight,

$$g_G(k\theta) = \frac{1}{2\pi} \int dz \; W_G^2(z) \; j_0(k\theta \, r) \quad (8)$$

where j_0 is the zero-th order Bessel function, and $r(z)$ denotes differential comoving distance, $dr = dz/H(z)$. In our analysis, we use $P(k) = 9.5 \times 10^5 k/(1 + (k/0.03)^2)^{1.2}$ which gives a good match to the measure w_{GG} in the APM with the above assumptions [2].

The temperature of CMB photons is gravitationally redshifted as they travel through the time-evolving dark-matter gravitational potential wells along the line-of-sight, from the last scattering surface $z_s = 1089$ to us today, $z = 0$ [29]. At a given sky position $\hat{\mathbf{n}}$:

$$\Delta T^{ISW}(\hat{\mathbf{n}}) = -2 \int dz \; \dot{\Phi}(\hat{\mathbf{n}}, z) \quad (9)$$

For a flat universe $\nabla^2 \Phi = -4\pi G a^2 \rho_m \delta$ (see Eq.[7.14] in [25]), which in Fourier space reads, $\Phi(k, z) = -3/2 \Omega_m \, (H_0/k)^2 \, \delta(k, z)/a$. Thus:

$$w_{TG}^{ISW}(\theta) \; = \; < \Delta_T^{ISW} \delta_G > = \int \frac{dk}{k} \; P(k) \; g(k\,\theta) \quad (10)$$

$$g(k\theta) \; = \; \frac{1}{2\pi} \int dz \; W_{ISW}(z) \; W_G(z) \; j_0(k\theta \, r)$$

where the ISW window function is given by $W_{ISW} = -3 \, \Omega_m \, (\frac{H_0}{c})^2 \, \dot{F}(z)$, with $c/H_0 \simeq 3000h$ Mpc^{-1} the Hubble radius today. $\dot{F} = d(D/a)/dr = (H/c)D(f-1)$ with $f \simeq \Omega_m^{6/11}(z)$ quantifies the time evolution of the gravitational potential. Note that $\dot{F}$ decreases as a function of increasing redshift (as $\Omega_m(z) \rightarrow 1$). It turns out that for flat universes, $\Omega_m + \Omega_\Lambda = 1$, W_{ISW} has a maximum a function of Ω_Λ and tends to zero both for $\Omega_\Lambda \rightarrow 1$ (since the prefactor $\Omega_m \rightarrow 0$) and also for $\Omega_\Lambda \rightarrow 0$ (because $\dot{F} \rightarrow 0$). The maximum ISW contribution to w_{TG}, for a fixed power spectrum, turns out to be at $\Omega_\Lambda \simeq 0.6$, closed to the current concordance model, but $\Omega_\Lambda \simeq 0.4 - 0.8$ give very similar results. This prediction is shown as a short-dashed line in Fig 3. Flat models which produce late time acceleration without a cosmological constant do not have these restrictions and can produce large values of $\dot{F}$ for a fixed Ω_m [23], such as Quintessence [34].

For the thermal Sunyaev-Zeldovich effect, we just assume that the gas pressure δ_{gas} fluctuations are traced by the APM galaxy fluctuations $\delta_{gas} \simeq b_{gas} \, \delta_G$ with an amplitude $b_{gas} \simeq 2$, representative of galaxy clusters. Note

that analytical results based on halo models and hydro-dynamic simulations show that this "gas bias" factor is scale and redshift dependent [27]. However, for low-z sources and linear scales one can safely take $b_{gas} = 2-4$. Thus a rough conservative estimate is given by [26]:

$$w_{TG}^{SZ}(\theta) = -b_{gas} \; \overline{\Delta T} w_{GG}(\theta) \quad (11)$$

where $\overline{\Delta T}$ is the SZ fluctuation amplitude sample by the APM, typically $\overline{\Delta T} \simeq 3\mu$K corresponds to a Compton parameter $y \simeq 4 \times 10^{-7}$ [26]. This prediction is shown as a long-dashed line in Fig 3. The total contribution $w_{TG} = w_{TG}^{ISW} + w_{TG}^{SZ}$ is shown as a continuous line.

IV. DISCUSSION

The main result of this paper is a measurement of a positive cross-correlation $w_{TG} = 0.35 \pm 0.20\mu$K (90% C.L.) between WMAP CMB temperature anisotropies and the Galaxy density fluctuations in the largest scales of the APM galaxy survey, $\theta \simeq 5 - 10°$. Large-scale modes from the primary SW temperature anisotropies introduce large sampling variance and makes measurements of the ISW contribution intrinsically noisy. The measured cross-correlation on $\theta > 5°$ scales is in good agreement, though a bit larger, than the predicted ISW effect for standard ΛCDM models (see Fig 3). For the measured APM $P(k)$ with $\sigma_8 \simeq 0.9$ and $b \simeq 1$, the ISW effect gives: $w_{TG} = 0.15\mu$K for flat universes with $\Omega_\Lambda = 0.4 - 0.8$. Flat models with $\Omega_\Lambda > 0.9$ or $\Omega_\Lambda < 0.2$ are ruled out at C.L. $> 95\%$. If such large ISW value is confirmed by future surveys, this observation would favor cosmological models that produce stronger linear growth suppression than the cosmological constant for a fixed Ω_m (eg. [23]), such as Quintessence [34].

If the detected cross-correlation is only due to the ISW effect [7], one would expect a stronger ISW-induced correlation on smaller scales (see Fig 3). Instead, on scales $\theta < 1°$, the measured mean cross-correlation becomes negative, $w_{TG} \approx -0.2 \pm 0.2\mu$K. This negative signal can be understood as thermal SZ contribution from hot gas in galaxy clusters [26]. Ignoring lensing, the SZ effect is contributing to a maximum level of $w_{TG}^{SZ} = w_{TG} - w_{TG}^{ISW} \approx -0.5 \pm 0.2 \pm 0.2\mu$K (90% C.L.). The two errors reflect the combined uncertainties at large and small scales. This imposes an upper bound on the mean Compton scattering of CMB photons crossing clusters on its way to the observer $y \lesssim 10^{-6}$, assuming the above model uncertainties (see also [8]).

Despite the fact that the APM is a high galactic latitude survey ($b < -40°$), our estimate of the SZ-induced cross-correlation can potentially be affected by Galactic dust contamination, which typically introduces a negative signal (see e.g. [24]). The amplitude of such cross-correlation would strongly depend on the WMAP band used for the analysis. In contrast, we find no differences between WMAP V and W-bands (see Fig 2).

By inspecting Fig 1 one can read off individual contributions from the ISW and SZ effects. On larger scales the product between APM and WMAP maps shows a clear correlation with the APM structure, while on smaller scales (right panel) this correlation fades away and turns into anticorrelation at the core of most APM clusters. The largest structures shown in the APM maps correspond to the very large scale potentials hosting superclusters or a few large clusters in projection. Some of these APM structures appear to be anti-correlated in the product map, but with very similar shapes (regions pointed by an arrow in Fig 1). This can be understood if we recall that the ISW is only a small part of the temperature anisotropies in the sky. Large scale modes from primordial SW fluctuations dominate over the secondary ISW anisotropies. This mostly contributes to the cosmic noise. But if a real (positive amplitude) ISW signal is "mounted" over a larger scale SW mode (of negative amplitude) it can still appear as a negative correlation in the cross-correlation map.

Our findings seem in agreement with recent work on the cross-correlation measure of WMAP with NRAO VLA Sky Survey radio source catalogue (NVSS) [6], [24]. They detect a signal of $w_{TG} \simeq 0.16\mu K$ with $1.8°$ pixels (148 counts/pixel), which is right at the level of the theoretical ISW prediction we estimate (see §3), and it is consistent with, but on the low end of, our measurements. The NRAO sources provides an almost 50% sky coverage (40% with the Kp0 WMAP mask), about 4 times the APM area, but the signal to noise is not 2 times better. First of all the selection function of NVSS is not well known, it consists of both nearby and very distance objects. The dominant peak seems at higher redshifts $z > 1$, which is less sensitive to ISW. Second the clustering is uncertain and affected by unknown artifacts, e.g. the mean source density seems to vary with declination [5]. Finally, NVSS has a very poor resolution (over one degree as compared to arcsecs in the APM). In summary, despite the potential advantage in total survey area, it is still unclear how well NVSS sources can trace the large scale structure of the universe. On the contrary, as its been extensively shown over the last 15 years, the APM has produced important tests of the gravitational instability picture and it has also been extensively cross-checked against other major surveys (see §I).

Thanks to the new generation of surveys, we can address new challenging questions to the cosmological model. Our cross-correlation analysis reveals that the evolution of the gravitational potential has been strongly suppressed at low redshift. We have also set new bounds on the SZ-induced distortion of CMB photons by clusters in the local universe. Deep large area galaxy surveys, such as the SDSS, should be able to confirm these results, provide tighter constraints on cosmological parameters and improve our knowledge of cluster physics [28]. Such analysis, together with a better modeling of the SZ and lensing effects will be presented elsewhere [11].

Acknowledgments

[1] Baugh C. M., Efstathiou G., 1993, MNRAS, 265, 145
[2] Baugh C. M., Gaztanaga E., 1996, MNRAS, 280, 37
[3] Bennett, C. L. et al. 2003, astro-ph/0302207
[4] Bennett, C. L., et al. 2003, ApJ, submitted
[5] Boughn, S. P. & Crittenden, R. G. 2002, PRL, 88, 21302
[6] —. 2003, astro-ph/0305001
[7] Crittenden, R. G., Turok, N., 1996, PRL, 76, 575
[8] Diego, J.M., Silk, J., Sliwa,W., 2003, astro-ph/0302268
[9] Dodelson, S. et al. 2002, ApJ, 572, 140
[10] Efstathiou, G., Sutherland, W. J., & Maddox, S. J. 1990, Nature (London) , 348, 705
[11] Fosalba P., Gaztañaga E., Castander F., in preparation
[12] Frieman J. A., Gaztañaga E., 1999, ApJ, 521, L83
[13] Gaztañaga, E. 2002, MNRAS, 333, L21
[14] —. 2002, ApJ, 580, 144
[15] —. 1995, ApJ, 454, 561
[16] —. 1994, MNRAS, 268, 913
[17] Gaztanaga E., Baugh C. M., 1998, MNRAS, 294, 229
[18] Gaztañaga E., Juszkiewicz R., 2001, ApJ, 558, L1
[19] Gaztañaga E., et al., astro-ph/0304178
[20] Górski, K. M., Hivon, E., & Wandelt, B. D. 1998, in Evolution of Large-Scale Structure: From Recombination to Garching
[21] Hinshaw, G. F. et al. 2003, ApJ, submitted
[22] Maddox, S. J., Efstathiou, G., Sutherland, W. J., & Loveday, J. 1990, MNRAS, 242, 43P
[23] Multamäki T., et al. MNRAS in press. astro-ph/0303526
[24] Nolta M.R., et al., astro-ph/0305097
[25] Peebles, P. J. E. 1980, The Large-Scale Structure of the Universe (Princeton, NJ: Princeton University Press)
[26] Refregier, A., Spergel D. N., Herbig T., 2000, ApJ, 531, 31
[27] Refregier, A., Teyssier, R., 2002, PRD, 66, 43002
[28] Peiris. H., Spergel, D.N., 2000, ApJ, 540, 605
[29] Sachs, R. K. & Wolfe, A. M. 1967, ApJ, 147, 73
[30] Scranton, R. et al. 2002, ApJ, 579, 48
[31] Seljak, U. & Zaldarriaga, M. 1996, ApJ, 469, 437
[32] Spergel, D. N. et al. 2003, astro-ph/0302209
[33] Szapudi I., Dalton G. B., Efstathiou G., Szalay A. S., 1995, ApJ, 444, 520
[34] Wang, L. & Steinhardt, P., 1998, ApJ 508, 483